



# Evaluation of bone perfusion during open orthopedic surgery using quantitative dynamic contrast-enhanced fluorescence imaging

I. LEAH GITAJN,<sup>1,4</sup> JONATHAN T. ELLIOTT,<sup>2,3</sup> JASON R. GUNN,<sup>3</sup>  
ALBERTO J. RUIZ,<sup>3</sup> ERIC R. HENDERSON,<sup>1</sup> BRIAN W. POGUE,<sup>3</sup>   
AND SHUDONG JIANG<sup>3,5</sup> 

<sup>1</sup>Department of Orthopaedics, Dartmouth-Hitchcock Medical Center, 1 Medical Dr., Lebanon, NH 03766, USA

<sup>2</sup>Department of Surgery, Dartmouth-Hitchcock Medical Center, 1 Medical Dr., Lebanon, NH 03766, USA

<sup>3</sup>Thayer School of Engineering, Dartmouth College, 14 Engineering Dr. Hanover, NH 03755, USA

<sup>4</sup>Ida.Leah.Gitajn@hitchcock.org

<sup>5</sup>Shudong.jiang@dartmouth.edu

**Abstract:** In this study, an indocyanine green (ICG)-based dynamic contrast-enhanced fluorescence imaging (DCE-FI) technique was evaluated as a method to provide objective real-time data on bone perfusion using a porcine osteotomy model. DCE-FI with sequentially increasing injury to osseous blood supply was performed in 12 porcine tibias. There were measurable, reproducible and predictable changes to DCE-FI data across each condition have been observed on simple kinetic curve-derived variables as well variables derived from a novel bone-specific kinetic model. The best accuracy, sensitivity and specificity of 89%, 88% and 90%, have been achieved to effectively differentiate injured from normal/healthy bone.

© 2020 Optical Society of America under the terms of the [OSA Open Access Publishing Agreement](#)

## 1. Introduction

Adequate vascular perfusion of bone and soft tissue is critical for healing as well as for prevention and management of surgical site infection following traumatic injury [1–8]. Adequate blood flow is needed to deliver nutrients, oxygen, growth factors, endogenous immune cells, and systemic antibiotics to injured tissues. The cornerstone of treatment of open contaminated fractures and/or established infections is a thorough surgical debridement of all devitalized or hypoperfused bone and soft tissue [9,10]. However, trauma surgeons currently have no objective tools available that can provide information on bone viability and therefore guide decision-making about the extent of debridement needed. Surgeons are therefore at risk of debriding too much or too little, both of which have profound clinical consequences.

At present, visual inspection by the surgeon remains the primary means of assessing bone viability or bone perfusion. Clinical signs of devitalized or poorly perfused bone include soft tissue stripping off bone (indicating a disruption to the periosteal blood supply), changes in bone color and lack of bleeding with multiple drill holes (termed the ‘paprika sign’) [11,12]. The subjective and imprecise nature of these assessments, which currently represent the ‘gold standard’, lead to substantial variation in treatment. Furthermore, the absence of an objective measure of bone perfusion has made it difficult to empirically define what an ‘aggressive’ or ‘thorough debridement’ actually means quantitatively.

The aim of this study was to evaluate whether indocyanine green (ICG)-based dynamic contrast-enhanced fluorescence imaging (DCE-FI), which has been used for decades in the operating room to assess vascular perfusion of tissues in several different fields such skin and perfusion imaging in plastic surgical indications and characterizing tumors in oncologic surgery, can provide an objective measurement of bone perfusion that is reproducible, predictable, robust,

and can differentiate ‘injured’ from ‘normal/healthy’ bone. We hypothesized that ICG-based DCE-FI would fulfill these criteria as an objective and evaluative tool for measuring bone perfusion.

## 2. Materials and methods

### 2.1. Animal experiments

This study was approved by our center’s Institutional Animal Care and Use Committee (IACUC) and conducted with research veterinarians. A total of six Yorkshire pigs (twelve tibias) weighing  $23 \pm 3$  Kg, were anesthetized with vital signs monitoring. The operative limbs were shaved with electric clippers. A longitudinal incision was made over the tibia. Dissection was carried down to the tibia, exposing the entire length of the tibia, taking care to keep the periosteum intact. The saphenous vein and artery were identified and protected in close proximity to the tibia.






Five sequential tibial conditions designed to model increasing severity in extremity trauma, were used in this study, and which are thought to correspond to increasingly severe disruption to the blood supply of the injured bone. Bone receives blood supply endosteal and periosteal sources. Endosteal blood flow is derived from the medullary artery in the medullary canal, which sends branches to the cortex and exhibits slower compartmental kinetics; periosteal blood flow is derived the periosteum and soft tissue envelope around the bone [13,14], and is and is characterized by faster, capillary phase kinetics.

In the context of traumatic injury, a simple fracture is associated with a break in the bone (disrupting endosteal blood flow) without any periosteal or soft tissue stripping (maintenance of periosteal blood flow) is relatively non-severe. With increasing fracture severity, there is increasing periosteal or soft tissue stripping or degloving, which additionally disrupts periosteal blood supplies [8,15]. With increasing injury severity (or increasing bony comminution and soft tissue stripping), the risk of complication such as infection or nonunion (non-healing fracture) rises significantly. This is thought to be related to the increasingly severe injury to the bone blood flow.

In 10 porcine tibias, five conditions were designed to model fracture with increasingly greater severity (Table 1). Time series of fluorescence images were acquired in each of the five clinically relevant conditions: (1) baseline, representing normal bone; (2) osteotomy of a 2 cm segment of the tibial diaphysis, representing a simple fracture, which is thought to disrupt the endosteal blood flow; (3) circumferential periosteal/soft tissue stripping of 2 cm of the proximal tibia, starting at the osteotomy (disrupting periosteal blood supply to that region, modelling a fracture with increasing soft tissue stripping, which is thought to disrupt periosteal blood flow; (4) circumferential periosteal/soft tissue stripping of the entire proximal tibia, modelling fracture with further increased severity/increased soft tissue stripping, which is thought to further disrupt periosteal blood flow; (5) circumferential periosteal/soft tissue stripping of the entire tibia (proximal and distal to the osteotomy), modelling extremely severe injury with extensive periosteal degloving, understood to severely disrupt periosteal blood flow. By design, we do expect prior conditions to affect subsequent conditions, as we are modelling fractures with increasing severity/energy transfer.

Although clinically, we would not be concerned about soft tissue stripping without a fracture (or osteotomy)—mechanistically, the fracture (or osteotomy) occurs in tandem with soft tissue stripping—in order to critically evaluate the endosteal contribution to bony blood flow as reflected in ICG-based DCE-FI, two additional porcine tibias underwent a different sequence of conditions: (I) baseline, (II) ~3 cm circumferential soft tissue stripping (disrupting periosteal blood supply but leaving endosteal blood supply completely intact), and (III) two diaphyseal osteotomies, separating this 3 cm of tibia (disrupting both periosteal and endosteal blood supply). At each condition, ICG kinetics was imaged 20 seconds and 4 minutes before and after ICG injection.

**Table 1. Porcine model with five clinically relevant conditions.**

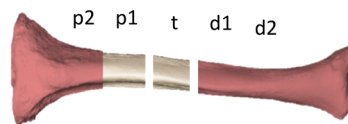
Condition	Surgical Description	Blood Supply Affected	Diagram
1	Baseline	/	
2	Osteotomy, creating a 2cm segment of diaphyseal bone with circumferential soft tissue stripping	1. Disrupts periosteal and endosteal blood supply from osteotomized bone 2. Disrupts endosteal blood supply to proximal and distal to osteotomy	
3	Circumferential periosteal/soft tissue stripping of 2cm of the proximal tibia, starting at the osteotomy	Disrupts periosteal blood supply proximal to osteotomy	
4	Circumferential periosteal/soft tissue stripping of entire proximal tibia, starting at the osteotomy	Disrupts periosteal blood supply proximal to osteotomy	
5	Circumferential periosteal/soft tissue stripping of the entire tibia (proximal and distal to the osteotomy)	Disrupts periosteal blood supply proximal and distal to osteotomy	

In the diagram, the white two lines indicate the location for osteotomy; the red and grey surfaces represent the bone with and without periosteal blood supply, respectively.

## 2.2. Dynamic contrast-enhanced fluorescence imaging

For each condition, ICG-based DCE-FI images were captured by a fluorescence surgical imaging system (Pentero, Zeiss and Spy Elite, Stryker). In these imaging systems, LED light sources in the wavelength ranges from 700 to 780 nm (of Pentero) and 805 nm (of Spy Elite) were used for excitation and the fluorescence lights in the wavelength range from 820 to 900 nm were detected by a CCD camera. The working distance was approximately 300 mm in all cases, and light intensity and integration times were kept constant for each device in each case. In each condition, 0.1 mg/kg ICG was injected intravenously. The dynamic fluorescence change was captured 20 seconds and 4 minutes before and after ICG injection, respectively. A total of 20 minutes was allowed for elimination of residual ICG between ICG injections. Pentero was used for the first 10 tibias and Spy Elite was used for the eleventh and twelfth tibias with the different three conditions than that involved in the first 10 tibias.

There were five regions of interest (ROIs) studied (Fig. 1): one ROI (t) is at the location of the osteotomy, two ROIs each at proximal (p1 & p2) and distal (d1 & d2), respectively. The length along each ROI is approximately 1 cm. For each of ROI, ICG intensity of all pixels inside of the ROI was averaged at each time point.

**Fig. 1.** Regions of interest.

Images acquired with the Pentero or Spy Elite were transferred to a local PC and processed using in-house developed MATLAB (TheMathWorks, Natwick, MA) software. The default integration times for each system was used, which was 5 fps and 2.75 fps for the Pentero and Spy Elite, respectively. Data associated with each ICG injection was converted to “change in

fluorescence” by subtracting the median of the first 5 seconds. Subsequent calculations are performed on this data.

### 2.3. Kinetic analysis

In addition to the maximum ICG intensity ( $I_{\max}$ ), which is a surrogate of perfusion, kinetic analysis was performed on the dynamic ICG fluorescence curves to quantify perfusion. An approach that accounts for the time-dependent hemodynamics attributed to the structure of bone blood supply, and has been described previously [16], was used. Briefly, the approach is based on the convolution theory of tracer kinetics, and is summarized graphically in Fig. 2. The measured tissue concentration curve,  $Q(t)$ , which is determined for each pixel of the time-series of images, is a convolution of  $C_a(t)$ , the time-concentration curves for the arterial blood (also called arterial input function [17]), and  $FR(t)$ , the impulse residue function.  $R(t)$  is mathematically defined as the fraction of remaining ICG in the tissue at time,  $t$ , following an idealized bolus (i.e., a temporal-delta function)).

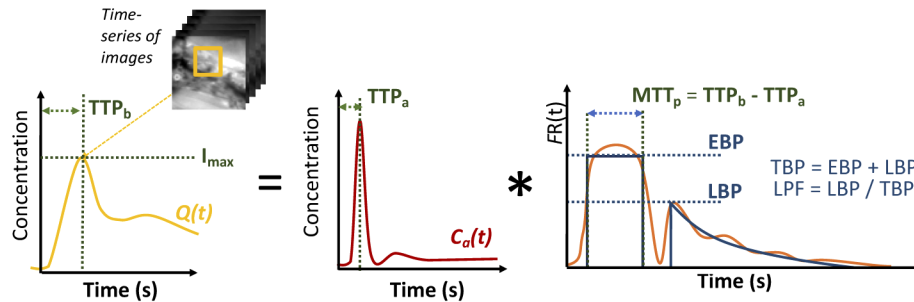


**Fig. 2.** Model of assessing bone perfusion using DCE-FI

A model-based approach involves parameterizing  $R(t)$  and fitting to recover those parameters; one of the most common models is the adiabatic approximation to the tissue homogeneity (AATH) [18] employed in CT Perfusion software. In this study, we modified AATH method to a hybrid plug-compartment (HyPC) to allow separate transit times for the fast and slow compartments [16]. The rationale for this modification, explained more extensively in a previous publication [16], is that since different arterial branches supply the periosteum and endosteal compartments, allowing separate arrival and transit times in the HyPC  $FR(t)$  function enables the recovery of a faster blood perfusion component we term ‘early bone perfusion’ (EBP, in units of mL/min/100 g), and a slower ‘late bone perfusion’ component (LBP, in units of mL/min/100 g), and the zero<sup>th</sup> statistical moment, mean transit time (MTT<sub>p</sub>). We further define the sum of EBP and LBP the total bone perfusion (TBP), and the fraction of LBP to TBP as late perfusion fraction (LPF). It should be noted that we have updated this terminology from our previous publication [16] to reflect the dynamic and not anatomic basis for the separation of components.

### 2.4. Statistical analysis and classification by machine learning

The mean and standard deviations from the first 10 tibias that were imaged by the Pentero were used for statistical analysis and classification by machine learning. The ROIs were classified as representing either injured or normal bone. Injured bone was defined as bone in regions directly affected by either cutting or stripping, as well as regions identified as being distal to the nutrient vessel severed by the transection. An unpaired two-sample Student t tests with unknown population standard deviations were used to estimate P-values, for the differences between injured and normal bone ROI for each variable. The data from 40 injured and 42 normal ROIs were used for the analysis. The unpaired two-sample test was used in this study was due to the sample

sizes were not equal in the two groups of ROIs. A P-value of .05 or less was considered to be significant for differences between the comparisons of groups evaluated. Receiver operating characteristic (ROC) curves were formed and area under the ROC curve (AUC) was obtained to illustrate graphically the performance of each variable.

For classification into normal and injured bone, a number of different variables from Fig. 2, in addition to intensity, time-to-peak, were examined, with  $I_{\max}$ , TBP, and LPF being identified as the most important features. A supervised learning model was trained and evaluated [19]. Total bone perfusion was plotted against late perfusion fraction (LPF), and grouped according to injured or normal bone labels described above. The boundary between these two clusters was determined using a linear Support Vector Machine (SVM) analysis [20]. The optimal hyperplane that separates the data into two classes was found by maximizing the margin between the plane and observations, and imposing a penalty for every observation on the wrong side of its class boundary. This optimization was carried out by the sequential minimal optimization routine [21]. The diagnostic ability of the model was evaluated using the leave- $p$ -out cross validation (LpOCV) approach, where 80% of the data was used to train the SVM and it was evaluated on the remaining 20% of the data. It has to note that this approach may be biased due to the limited sample size.

### 3. Results

The results of this study demonstrated measurable, reproducible and predictable differences in ICG-based DCE-FI parameters in each region of interest through each sequential condition using simple kinetic-curve derived variables and hemodynamic-modelling derived variables. Figure 3 shows an example of the fluorescence images and change in fluorescence curves from one porcine tibia. The ICG fluorescence map overlay on white light bone images as well as dynamic change in fluorescence curves at the proximal and distal regions of interest (ROI, green (p2) and blue (d2)), through each condition outlined in Table 1. To enhance visualization, the transparency of fluorescence information was increased in non-bone portions of the image. The vertical axes of the curves are the ICG intensity with arbitrary fluorescence units. The dynamic change in fluorescence curves represent the raw data after smoothing with a 10-sec frame, 3rd-order Savitzky-Golay filter (black dots), and the result of fitting these curves with the HyPC model (blue line). The ICG maximum fluorescence intensity ( $I_{\max}$ ) and temporal dynamic curves of ICG kinetics change substantially across conditions and regions of interest (ROIs). Baseline conditions, (see column (1)) without disruption of either periosteal or endosteal blood supply demonstrated the highest  $I_{\max}$ . Similarly, the next highest  $I_{\max}$  was noted in ROIs proximal and distal to the osteotomy, prior to any removal of periosteum (leaving periosteal blood supply intact with endosteal blood flow partially disrupted as a result of the osteotomy) (see column (2)). As sequential soft tissue stripping was performed, the ICG intensity decreased due to sequentially removing periosteal blood supply (see columns (3) & (4)). The osteotomized fragment of bone, with both periosteal and endosteal blood supply disrupted, demonstrated the lowest ICG intensity and a flat dynamic curve (see column (5)). The overall curve shape changes with progressive injury to endosteal and periosteal blood supplies, as well. All images of other 9 tibias are similar to this example.

Figure 4 demonstrates the change in  $I_{\max}$  at each ROI in each condition, which reflects a dose-response curve-type effect of sequential injury to osseous blood flow at each region of interest. As shown in Fig. 4, at ROI t, when a 2 cm segment of bone was osteotomized and stripped of periosteum/soft tissue circumferentially, there was a statistically significant drop in  $I_{\max}$  from 210 to 31, and then  $I_{\max}$  in this ROI remained at the low level for the remainder of the study. The next most proximal segment (ROI p1) demonstrated the step drops following the osteotomy, soft tissue/periosteum was stripped off this region of interest, and soft tissue/periosteum was stripped off the entire proximal segment of bone. The similar trend can be seen in the further proximal

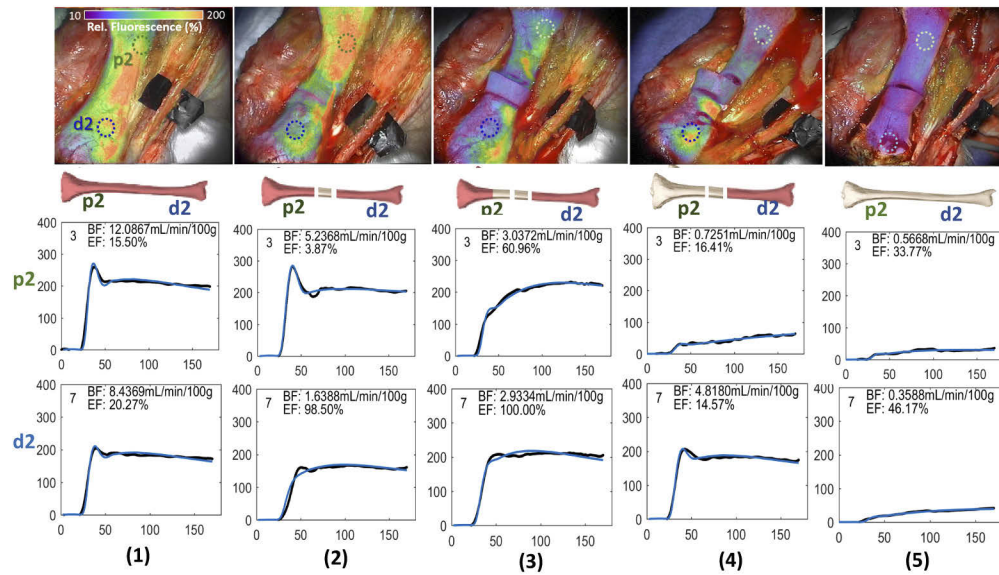


**Fig. 3.** The images and change in fluorescence curves associated with one representative porcine tibia. ICG fluorescence map overlay on the white light images as well as temporal dynamic curves of the ICG kinetics in two regions of interest (most proximal (p2, green) and most distal (d2, blue), shown in each image) at (1) baseline, (2) osteotomizing a 2 cm segment of bone, (3) 2 cm soft tissue/periosteal stripping proximal to the osteotomy, (4) complete soft tissue/periosteal stripping proximal to the osteotomy, (5) complete soft tissue/periosteal stripping proximal and distal to the osteotomy. To enhance visualization, the transparency of fluorescence information was increased in non-bone portions of the image. The dynamic change in fluorescence curves represent the raw data after smoothing with a 10-sec frame, 3rd-order Savitzky-Golay filter (black dots), and the result of fitting these curves with the HyPC model (blue line).

segment of bone (ROI p2). In ROIs just distal to the osteotomy (d1), the osteotomy reduced  $I_{\max}$  to about half from a baseline of 90, and further reduced to almost 0 when the entire distal segment was stripped of periosteum and soft tissue.  $I_{\max}$  changes in the further distal ROI (d2) had the very similar trend as that in ROI d1, demonstrate  $I_{\max}$  changes were due to the condition change but not the ROI location changes.

The methodology for 11<sup>th</sup> and 12<sup>th</sup> tibias was designed to assess the effect of disruption of periosteal blood supply in isolation, prior to disruption of endosteal blood supply. Figure 5 demonstrates the kinetic curves associated with ICG fluorescence in the ROI of 11<sup>th</sup> tibia (grey shadowed position in Legend of (b)) in each condition of (I) baseline (red), (II) ~3 cm circumferential soft tissue stripping (blue) and (III) two diaphyseal osteotomies, separating this 3 cm of tibia (black). For better understanding the kinetic curve change due to the different bone damages, the kinetic curves plotted in two ways: (a) ICG intensity after subtracting the average values of ICG before each injection, and (b) ICG intensity normalized by the maximum ICG value in each condition. As shown in Fig. 5(a), maximum ICG intensity decreased 50% from baseline when soft tissue was stripped from the bone (disrupting the periosteal blood supply in isolation) and 98% from baseline when the bone was osteotomized (adding disruption of the endosteal blood supply, bottom black curve), as expected. As shown in Fig. 5(b), when soft tissue is stripped, not only is the maximum intensity reduced, but also the time required to reach to the maximum point is longer than in baseline. This suggests EBP is mainly sensitive to periosteal blood supply damage. ICG fluorescence maps at each condition are shown in Supplemental

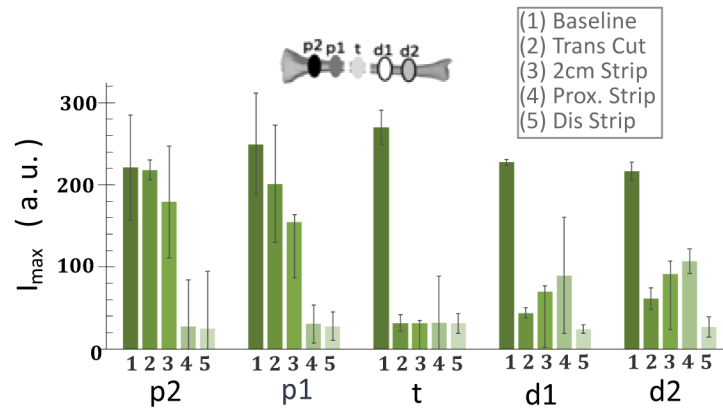


**Fig. 4.**  $I_{\max}$  in each region of interest at (1) baseline, (2) osteotomizing a 2 cm segment of bone, (3) 2 cm soft tissue/periosteal stripping proximal to the osteotomy, (4) complete soft tissue/periosteal stripping proximal to the osteotomy, (5) complete soft tissue/periosteal stripping proximal and distal to the osteotomy.

Figure 1 in [Supplement 1](#). To enhance visualization, the region corresponding to the bone only was segmented from the surrounding soft tissue, using white light images as a guide. A video of the real time fluorescence imaging of the baseline of this tibia are shown in [Visualization 1](#). The kinetic curve and images of the 12<sup>th</sup> tibia had the same trend and images as it shown in this Fig. 5.

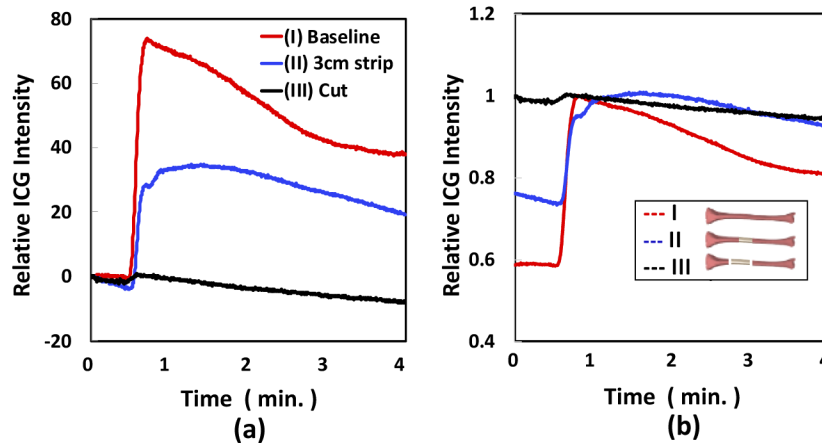


**Fig. 5.** ICG kinetics in ROI (grey shadowed position in legend of (b)) at different conditions of (I) baseline (red), (II) ~3 cm circumferential soft tissue stripping (blue) and (III) two diaphyseal osteotomies, separating this 3 cm of tibia (black). (a) ICG intensity after subtracting the average values of ICG before each injection, (b) ICG intensity normalized by the maximum ICG value in each condition.

When ROIs in the first 10 legs were classified as representing either injured or normal (healthy) bone, the boxplots (a)-(c) and ROC curves (d) of using each of (a)  $I_{\max}$ , (b) TBP and (c) LPF as the indicator to differentiate injured from the normal bone, are shown in Fig. 6. In each box shown in Fig. 6(a)-(c), horizontal lines indicate median and vertical lines extending from the top and bottom of boxes represent range in data in each case. The values of TBP and LPF of injured and normal bone were significantly different while the values of  $I_{\max}$  in these two groups were somewhat overlapped. Figure 6(d) contains ROC analysis of sensitivity versus specificity as

quantified by the normalized AUC for  $I_{\max}$  (gold line), TBP (blue line with filled cycles) and LPF (black line with filled triangles). The higher than 0.5 AUC values for  $I_{\max}$ , TBP and LPF, indicating the potential for using these variables as the indicators to diagnose bone health with high sensitivity and specificity, during the orthopedic surgery.

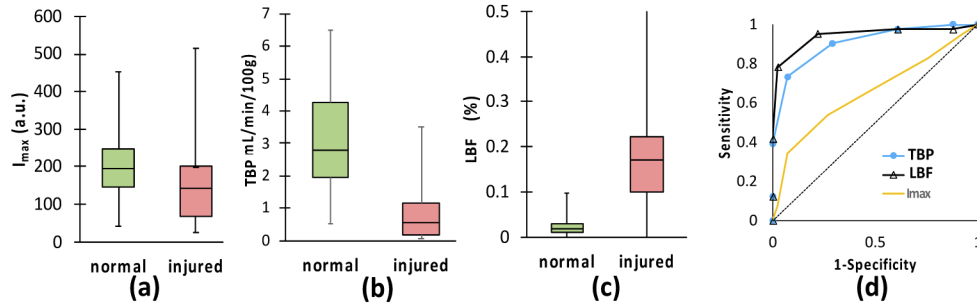


**Fig. 6.** Boxplots and ROC curves of using each of  $I_{\max}$ , TBP, and LBF as an indicator to differentiate injured from the normal bone.

Figure 7 shows SVM classification of injured and normal bone according to the combination of TBP and LPF. Red crosses and green cycles were the data from injured and normal bone ROIs, respectively. As the result, the two groups were clearly separated by the hyperplane (which is a 1-dimensional line in this case since the ambient space is the two-dimensional variable space), of  $LPF = 0.51 \cdot TBP - 0.72$ .

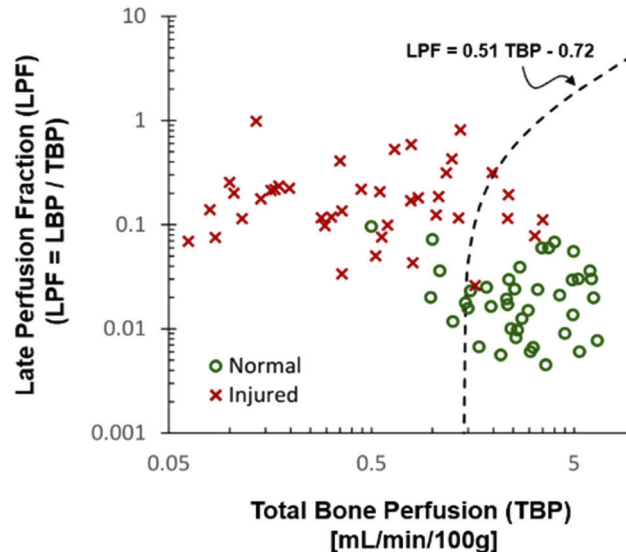


**Fig. 7.** SVM Classification of healthy and damaged bone according to TBP and LPF (%) values. Dashed line shows the decision boundary.

Table 2 summarizes the means, standard deviations (SDs), p-values, AUCs, sensitivities, specificities, and accuracies of using each of variable to differentiate injured from normal bone ROIs. The average  $I_{\max}$ , TBP and LPF were 163 a.u., 0.8 mL/min./100 g, and 21.4%, in ROIs of injured bone, whereas 201 a.u., 3.2 mL/min./100 g, and 2.5% in normal bone, respectively. Standard deviations (SD) in each category were 58 a.u., 0.8 mL/min./100 g, 10%, for injured bone ROIs; 50 a.u., 0.8 mL/min./100 g, and 1%, respectively. P-values of using each of  $I_{\max}$ , TBP



and LPF for differentiating the injured from normal bone were 0.12, <0.001, and <0.001. The AUC values were 0.64, 0.83 and 0.88 for  $I_{\max}$ , TBP and LPF, indicating the potential for using these variables as the indicators to diagnose bone health with high sensitivity and specificity, during the orthopedic surgery. Comparing to the signal variable of either  $I_{\max}$ , or TBP or LPF, the combination of TBP and LPF, with SVM classification demonstrated the best diagnostic performance in 89% accuracy, with the specificity of 88% and sensitivity of 90%, respectively.

**Table 2. Summary of the means, SDs, p-values, AUCs, sensitivities, specificities, and accuracies of using each of variable to differentiate injured from normal bone ROIs.**

	$I_{\max}$ (a.u.)	TBP	EBP	LBP	LPF (%)	TBP & LPF
		(mL/min./100 g)				
<b>Normal</b>	201 ± 50	3.2 ± 0.8	3.0 ± 0.8	0.1 ± 0.0	2.5 ± 1.1	/
<b>Injured</b>	163 ± 58	0.8 ± 0.4	0.7 ± 0.4	0.2 ± 0.1	21.4 ± 10.0	/
<b>p-value</b>	0.12	<0.001	<0.001	0.05	<0.001	/
<b>AUC</b>	0.65	0.83	0.85	0.64	0.97	/
<b>Sensitivity</b>	0.54	0.73	0.78	0.46	0.78	0.90
<b>Specificity</b>	0.73	0.93	0.98	0.66	0.98	0.88
<b>Accuracy</b>	0.63	0.83	0.88	0.56	0.88	0.89

#### 4. Discussion

This is the first study to apply fluorescence imaging to dynamically assess bone vascularity in real time. ICG-based fluorescence imaging for soft tissue blood perfusion related applications such as real-time intra-operative arterial and lymphatic perfusion imaging, [22,23] and osseous flap perfusion imaging [24], has been studied for more than a decade. In these applications, ICG images were used to define the blood perfusion qualitatively over a relatively homogenous tissue volume and simple blood flow system, under the reasonable sensitivity and dynamic range. We have adapted these fluorescence-based methods from these other fields to more complex orthopedic applications where intraoperative vascular perfusion assessment of bone is critically important but lacks objective and quantitative methods. This technology is based on use of an imaging system with high sensitivity and dynamic range to capture the ICG kinetic curve changes in bone and an analysis of the dynamic ICG inflow/outflow curve on a specific bone blood flow model. This data suggests that the faster early component of the kinetic curve (early bone perfusion or EBP) reflects periosteal blood flow while the slower late component of the kinetic curve (late bone perfusion or LBP) reflects the endosteal blood flow. The results from this study in a porcine model demonstrates that ICG-based DCE-FI can quantitatively measure bone perfusion from both superficial (periosteal) sources as well as deep (endosteal) sources, with predictable and reproducible changes following sequential sacrifice of osseous bone perfusion sources. This study demonstrated that kinetic analysis of the dynamic ICG inflow/outflow curve can differentiate hypo-perfused bone with a high degree of accuracy (TBP + LPF with sensitivity, specificity and accuracy of 90%, 88% and 89% respectively). This work suggests that ICG-based DCE-FI has potential to provide surgeons with an objective measure of bone vascularity in real-time that will improve objectivity and reduce variability associated with surgical management of traumatic injury and infection.

Adequate perfusion is critical to maintenance bone strength, remodeling, prevention of fracture, bony ingrowth into arthroplasty implants, fracture repair/healing and preventing and treating infection [4–8]. Changes in bone blood flow have been implicated in morbidity associated with tobacco smoke, osteoporosis, osteoarthritis, diabetes and development and persistence of bone infection [25–35]. The cornerstone of treatment of patients who have a bone infection or

osteomyelitis, in the setting of prior fracture or prior arthroplasty, is debridement or removal of all poorly perfused bone because devitalized bone will not be reached by systemic antibiotics or endogenous immune cells and, therefore, becomes a nidus for biofilm formation [36]. Similarly, in the setting of high energy open fractures, thoroughness of debridement of devitalized bone is thought to be the most important way to prevent complications such as infection or nonunion. In both of these settings, more extensive debridement is thought to minimize risk of treatment failure; however, this comes at the cost of increasingly complex reconstructive procedures to fill bony defects [37–39]. To date, there is no ‘gold standard’ means to assess bone perfusion in real time. In the current paradigm surgeons use visual and tactile clues to make a subjective assessment about bone viability and bone blood flow. The subjective and imprecise nature of this visual and tactile assessment leads to substantial variation in treatment and lack of advancement in objectively-driven treatment regimens. This study represents the first step toward adapting fluorescence-guided surgical principles to orthopedic applications. In this study ICG-based DCE-FI appeared to accurately reflect changes in bone perfusion in real time. Based on the result of this study, ICG-based DCE-FI data optimized for hemodynamic assessment of bone shows enormous promise as a technique that may help orthopedic surgeons make more objective and accurate assessments during infection and/or fracture surgery.

There are limitations associated with the present study. There is no “gold standard” imaging technique applicable to bone perfusion to compare ICG fluorescence imaging perfusion measurements with. However, our model utilized clinically relevant conditions in which endosteal blood supply was disrupted followed by sequential disruption in periosteal blood supply. In each condition, each region of interest demonstrated the anticipated ICG fluorescence response reflecting the surgical sequence. Additionally, there were a relatively small number of experimental animals, which is typical for large-animal models. However, despite this, we demonstrated highly reliable, reproducible and predictable differences in bone perfusion as measured by ICG fluorescence with sequential disruption of blood supply, each with statistical significance. Some of the modelling-derived variables demonstrated high variability with large error bars. It is likely that this is related to the modelling construct since the simple kinetic curve-derived variables demonstrated smaller error bars and less variability. However, it is possible that this reflects inherent differences in tibial blood flow between animals or differences in surgical procedure. This will be explored in more detail in future studies.

The present study demonstrated that ICG-based DCE-FI has the potential to be a reliable and reproducible technique to quantitatively measure bone perfusion. More research is needed to translate this research into a useful surgical guidance technology for human patients. Additional studies are also planned to determine how strong the association is between EBP and LBF is with periosteal and endosteal tissue, respectively, which would add additional value to clinical decision-making. Quantitative measurement of osseous and peri-osseous blood flow has the potential to revolutionize the standard of care for millions of patients with orthopedic conditions from civilian- and combat-related trauma to osteoporotic or geriatric fracture to diabetes to arthroplasty by providing clinicians with a simple tool that can be used to assess bone viability and potential for healing, remodeling, ingrowth onto implant surfaces and/or infection control.

## 5. Conclusion

Assessment of bone and tissue viability is an essential component of surgical decision-making. The results obtained from this first study to apply ICG-based DCE-FI to assess bone perfusion in an orthopedic setting, suggested that ICG-based DCE-FI can provide surgeons with an objective intraoperative measure of bone viability critical to optimizing treatment of patients who sustain injury. More research is needed to translate this research into an operational surgical guidance technology for human patients. Quantitative measurement of osseous and peri-osseous blood flow has the potential to revolutionize the standard of care for millions of patients with orthopedic

conditions from civilian- and combat-related trauma to osteoporotic or geriatric fracture to diabetes to arthroplasty by providing clinicians with a simple tool that can be used to assess bone viability and potential for healing, remodeling, ingrowth onto implant surfaces and/or infection control.

## Funding

National Institute of Biomedical Imaging and Bioengineering (K23EB026507); National Cancer Institute (K99CA190890); Dartmouth College (UL1TR001086).

## Acknowledgments

This work has been funded by a Dartmouth SYNERGY Grant (UL1TR001086) and salary support & training by NIH/NCI R00CA190890 (JTE) and NIH/NIBIB K23EB026507 (ERH). Authors have submitted US Provisional Patent Application No. 62/755,067 on the subject presented in this paper.

## Disclosures

The authors declare no conflicts of interest.

See [Supplement 1](#) for supporting content.

## References

1. N. D. Charkes, M. Brookes, and P. T. Makler Jr., "Studies of skeletal tracer kinetics: II. evaluation of a five-compartment model of [<sup>18</sup>F]fluoride kinetics in rats," *J Nucl Med* **20**, 1150–1157 (1979).
2. P. M. Gross, D. D. Heistad, and M. L. Marcus, "Neurohumoral regulation of blood flow to bones and marrow," *Am. J. Physiol.* **237**(4), H440–H448 (1979).
3. R. Wootton, J. Reeve, and N. Veall, "The clinical measurement of skeletal blood flow," *Clin. Sci. Mol. Med.* **50**(4), 261–268 (1976).
4. Y. Fujikawa, J. M. Quinn, A. Sabokbar, J. O. McGee, and N. A. Athanasou, "The human osteoclast precursor circulates in the monocyte fraction," *Endocrinology* **137**(9), 4058–4060 (1996).
5. I. B. Mazo and U. H. von Andrian, "Adhesion and homing of blood-borne cells in bone marrow microvessels," *J. Leukoc Biol.* **66**(1), 25–32 (1999).
6. C. Martin, P. C. Burdon, G. Bridger, J. C. Gutierrez-Ramos, T. J. Williams, and S. M. Rankin, "Chemokines acting via CXCR2 and CXCR4 control the release of neutrophils from the bone marrow and their return following senescence," *Immunity* **19**(4), 583–593 (2003).
7. G. Z. Eghbali-Fatoureechi, J. Lamsam, D. Fraser, D. Nagel, B. L. Riggs, and S. Khosla, "Circulating osteoblast-lineage cells in humans," *N. Engl. J. Med.* **352**(19), 1959–1966 (2005).
8. M. Marenzana and T. R. Arnett, "The Key Role of the Blood Supply to Bone," *Bone Res.* **1**(3), 203–215 (2013).
9. H. C. Yun, C. K. Murray, K. J. Nelson, and M. J. Bosse, "Infection After Orthopaedic Trauma: Prevention and Treatment," *J. Orthop. Trauma* **30**(Suppl 3), S21–S26 (2016).
10. M. Panteli and P. V. Giannoudis, "Chronic osteomyelitis: what the surgeon needs to know," *EFORT Open Rev.* **1**(5), 128–135 (2016).
11. G. Cierny 3rd, J. T. Mader, and J. J. Penninck, "A clinical staging system for adult osteomyelitis," *Clin. Orthop. Relat. Res.* **414**, 7–24 (2003).
12. B. Parsons and E. Strauss, "Surgical management of chronic osteomyelitis," *Am. J. Surg.* **188**(1), 57–66 (2004).
13. M. Brookes and W. J. Revell, *The Blood Supply of Bone: Scientific Aspects* (Springer, 1998).
14. H. Crook, *An Atlas of Vascular Anatomy of the Skeleton and Spinal Cord* (Dunitz Martin, 1996).
15. I. McCarthy, "The physiology of bone blood flow: a review," *J. Bone Joint Surg. Am.* **88**(Suppl 3), 4–9 (2006).
16. J. T. Elliott, S. Jiang, B. W. Pogue, and I. L. Gitajn, "Bone-specific kinetic model to quantify periosteal and endosteal blood flow using indocyanine green in fluorescence guided orthopedic surgery," *J Biophotonics* **4**, 206–218 (2019).
17. J. T. Elliott, R. R. Addante, G. P. Slobegean, S. Jiang, E. R. Henderson, B. W. Pogue, and I. L. Gitajn, "Intraoperative fluorescence perfusion assessment should be corrected by a measured subject-specific arterial input function," *J. Biomed. Opt.* **25**(06), 1–14 (2020).
18. K. S. St Lawrence and T. Y. Lee, "An adiabatic approximation to the tissue homogeneity model for water exchange in the brain: I. Theoretical derivation," *J. Cereb. Blood Flow Metab.* **18**(12), 1365–1377 (1998).

19. N. Christianini and J. C. Shawe-Taylor, *An Introduction to Support Vector Machines and Other Kernel-Based Learning Methods* (Cambridge University Press, 2000).
20. V. N. Vapnik, *The Nature of Statistical Learning Theory* (Springer-Verlag New York Inc., 2000).
21. R. E. Fan, P. H. Chen, and C. J. Lin, "Working set selection using second order information for training support vector machines," *J Mach Learn Res* **6**, 1889–1918 (2005).
22. R. A. Cahill, F. Ris, and N. J. Mortensen, "Near-infrared laparoscopy for real-time intra-operative arterial and lymphatic perfusion imaging," *Colorectal Disease* **13**, 12–17 (2011).
23. M. B. Reinhart, C. R. Huntington, L. J. Blair, B. T. Heniford, and V. A. Augenstein, "Indocyanine Green: Historical Context, Current Applications, and Future Considerations," *Surg. Innov.* **23**(2), 166–175 (2016).
24. I. Valerio, J. M. Green 3rd, J. M. Sacks, S. Thomas, J. Sabino, and T. O. Acarturk, "Vascularized osseous flaps and assessing their bipartate perfusion pattern via intraoperative fluorescence angiography," *J. Reconstr. Microsurg.* **31**(1), 45–53 (2014).
25. M. Laroche, I. Ludot, M. Thiechart, J. Arlet, M. Pieraggi, P. Chiron, L. Moulinier, A. Cantagrel, J. Puget, G. Utheza, and B. Mazieres, "Study of the intraosseous vessels of the femoral head in patients with fractures of the femoral neck or osteoarthritis of the hip," *Osteoporosis Int.* **5**(4), 213–217 (1995).
26. G. Bridgeman and M. Brookes, "Blood supply to the human femoral diaphysis in youth and senescence," *J Anat* **188**(Pt 3), 611–621 (1996).
27. D. A. Hanley, J. P. Brown, A. Tenenhouse, W. P. Olszynski, G. Ioannidis, C. Berger, J. C. Prior, L. Pickard, T. M. Murray, T. Anastassiades, S. Kirkland, C. Joyce, L. Joseph, A. Papaioannou, S. A. Jackson, S. Poliquin, J. D. Adachi, G. Canadian, and Multicentre Osteoporosis Study Research, "Associations among disease conditions, bone mineral density, and prevalent vertebral deformities in men and women 50 years of age and older: cross-sectional results from the Canadian Multicentre Osteoporosis Study," *J. Bone Miner. Res.* **18**(4), 784–790 (2003).
28. M. Sanada, A. Taguchi, Y. Higashi, M. Tsuda, I. Kodama, M. Yoshizumi, and K. Ohama, "Forearm endothelial function and bone mineral loss in postmenopausal women," *Atherosclerosis* **176**(2), 387–392 (2004).
29. I. D. McCarthy, "Fluid shifts due to microgravity and their effects on bone: a review of current knowledge," *Ann. Biomed. Eng.* **33**(1), 95–103 (2005).
30. E. J. Barrett and Z. Liu, "The endothelial cell: an "early responder" in the development of insulin resistance," *Rev. Endocr. Metab. Disord.* **14**(1), 21–27 (2013).
31. S. Rattigan, S. M. Richards, and M. A. Keske, "Microvascular contributions to insulin resistance," *Diabetes* **62**(2), 343–345 (2013).
32. J. N. Farr, M. T. Drake, S. Amin, L. J. Melton 3rd, L. K. McCready, and S. Khosla, "In vivo assessment of bone quality in postmenopausal women with type 2 diabetes," *J. Bone Miner. Res.* **29**(4), 787–795 (2014).
33. M. P. Gilbert and R. E. Pratley, "The impact of diabetes and diabetes medications on bone health," *Endocr. Rev.* **36**(2), 194–213 (2015).
34. L. Zhao, Z. Fu, J. Wu, K. W. Aylor, E. J. Barrett, W. Cao, and Z. Liu, "Inflammation-induced microvascular insulin resistance is an early event in diet-induced obesity," *Clin. Sci.* **129**(12), 1025–1036 (2015).
35. P. S. Hinton, "Role of reduced insulin-stimulated bone blood flow in the pathogenesis of metabolic insulin resistance and diabetic bone fragility," *Med. Hypotheses* **93**, 81–86 (2016).
36. A. Christersson, S. Larsson, and J. Sorensen, "Presurgical localization of infected avascular bone segments in chronic complicated posttraumatic osteomyelitis in the lower extremity using dual-tracer PET/CT," *EJNMMI Res.* **8**(1), 65 (2018).
37. H. Duman, M. Sengezer, B. Celikoz, M. Turegun, and S. Isik, "Lower extremity salvage using a free flap associated with the Ilizarov method in patients with massive combat injuries," *Ann. Plast. Surg.* **46**(2), 108–112 (2001).
38. D. W. Lowenberg, R. F. Buntic, G. M. Buncke, and B. M. Parrett, "Long-term results and costs of muscle flap coverage with Ilizarov bone transport in lower limb salvage," *J. Orthop. Trauma* **27**(10), 576–581 (2013).
39. C. Papakostidis, M. Bhandari, and P. V. Giannoudis, "Distraction osteogenesis in the treatment of long bone defects of the lower limbs: effectiveness, complications and clinical results; a systematic review and meta-analysis," *Bone Joint J.* **95-B**(12), 1673–1680 (2013).